Synthesis and Electrochemical and EPR Studies of Spiked Butterfly Metal Clusters Containing an Fe_3HgM Core (M = Mo, W, Fe, Mn, Co)

Roser Reina, Oriol Rossell,* and Miquel Seco

Departament de Química Inorgànica, Universitat de Barcelona, Diagonal 647, E-08028 Barcelona, Spain

Dominique de Montauzon

Laboratoire de Chimie de Coordination du CNRS, 205 Route de Narbonne, 31077 Toulouse Cedex, France

Rachid Zquiak

Departament de Física Fonamental, Universitat de Barcelona, Martí i Franqués 1, E-08028 Barcelona, Spain

Received April 25, 1994[⊗]

The reaction of the PPh_4^+ salt of $[Fe_3(CO)_{11}]^{2-}$ with ClHg(m) complexes (m = metal fragment) in tetrahydrofuran gives high yields of the new pentametallic clusters $(PPh_4)[Fe_3(CO)_{10}(\mu\text{-CO})(\mu\text{-Hg(m)})]$ (m = $Mo(CO)_3Cp$ (**1**), $W(CO)_3Cp$ (**2**), $Fe(CO)_2Cp$ (**3**), $Mn(CO)_5$ (**4**), $Co(CO)_4$ (**5**)) showing a spiked butterfly geometry, according to their IR, FAB, and Mössbauer spectra. These species are stable toward metal ligand redistribution processes. The electrochemical oxidation of these mixed transition metal−mercury clusters led to the paramagnetic species $[Fe_3(CO)_{11}(\mu\text{-Hgm})]^{\bullet}$, which have been identified by EPR spectroscopy. From those parameters it is deduced that the unpaired electron is mainly localized in the Fe_3Hg butterfly metallic core.

Introduction

The use of anionic carbonyl clusters for condensation reactions with gold(I) or mercury (II) salts has been shown to be a powerful method for the formation of mixed-metal clusters.[1,2] Recently, we have described the synthesis and structural characterization of some mixed iron−gold (or mercury) clusters by using the unsupported $[Fe_2(CO)_8]^{2-}$[3,4] or the Fe−Fe-supported anions $[Fe_2(CO)_6(\mu\text{-CO})(\mu\text{-L})]^-$ (L = PPh_2,[5] CPh_2 = CHPh,[6] S^iPr[7]) as building blocks. Thus, the anionic (**A**)- or the neutral triangular (**B**) frameworks have been

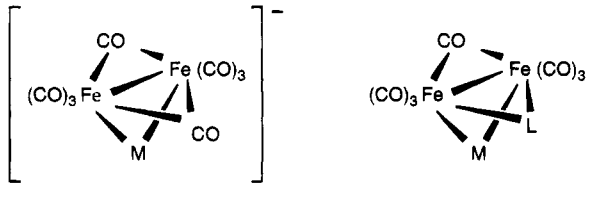

A **B**

M= Hgm, $AuPPh_3$

obtained. Considering the isolobal relationship between the species CO, PPh_2^+, and $Fe(CO)_4$, it seemed interesting to study the reaction of the related $[Fe_3(CO)_{11}]^{2-}$ anion with the bimetallic complexes ClHg(m) (m = a metal fragment, such as $Mo(CO)_3Cp$), in an attempt to obtain pentametallic clusters displaying an unusual Fe_3HgM spiked butterfly frame. In fact, we have just reported the synthess of $[Fe_3(CO)_{10}(\mu\text{-CO})(\mu\text{-AuPPh}_3)]$,[8] in which the metal core consists of an Fe_3Au butterfly arrangement. We were also interested in determining whether these transition metal−mercury clusters are stable toward metal ligand redistribution reactions. This kind of process is being extensively investigated for group-12 metals,[9] and although the factors which govern the reaction are still unclear, it appears that the negative charge delocalized over the unsymmetric cluster may favor its stabilization toward the symmetric derivative. In addition, taking into account the electrochemical behavior of the derivatives $Hg(m)_2$, it was anticipated that the new compounds could be suitable species for electrochemical studies. Indeed, the complexes $(PPh_4)[Fe_3(CO)_{10}(\mu\text{-CO})(\mu\text{-Hgm})]$ undergo a one-electron-oxidation process to give paramagnetic derivatives, which, although not isolated, have been detected by EPR spectroscopy.

[⊗] Abstract published in *Advance ACS Abstracts,* September 1, 1994.

(1) Salter, I. D. *Adv. Organomet. Chem.* **1989**, *29*, 249.
(2) Gade, L. H. *Angew. Chem., Int. Ed. Engl.* **1993**, *32*, 24.
(3) Rossell, O.; Seco, M.; Jones, P. J. *Inorg. Chem.* **1990**, *29*, 348.
(4) Alvarez, S.; Rossell, O.; Seco, M.; Valls, J.; Pellinghelli, M. A.; Tiripicchio, A. *Organometallics* **1991**, *10*, 2309.
(5) Ferrer, M.; Reina, R.; Rossell, O.; Seco, M.; Solans, X. *J. Chem. Soc., Dalton Trans.* **1991**, 347.
(6) Reina, R.; Rossell, O.; Seco, M.; Ros, J.; Yáñez, R.; Perales, A. *Inorg. Chem.* **1991**, *30*, 3973.
(7) Delgado, E.; Hernández, E.; Rossell, O.; Seco, M.; Gutierrez-Puebla, E.; Ruiz, C. *J. Organomet. Chem.* **1993**, *455*, 177.
(8) Rossell, O.; Seco, M.; Reina, R.; Font-Bardía, M.; Solans, X. *Organometallics* **1994**, *13*, 2127.
(9) See, for example: (a) Mays, M. J.; Robb, J. D. *J. Chem. Soc. A* **1968**, 329. (b) Rosenberg, E.; Rickman, D.; I-Nan Hsu; Geller, R. W. *Inorg. Chem.* **1986**, *25*, 194. (c) Rossell, O.; Seco, M.; Torra, I. *J. Chem. Soc., Dalton Trans.* **1986**, 1011. (d) Henly, T. J.; Shapley, J. R. *Organometallics* **1989**, *8*, 2729. (e) Gade, L .H.; Johnson, B. F. G.; Lewis, J.; McPartlin, M.; Powell, H. *J. Chem. Soc., Dalton Trans.* **1992**, 921. (f) Andreu, P. L.; Cabeza, J. A.; Llamazares, A.; Riera, V.; García-Granda, S.; Van der Maelen, J. F. *J. Organomet. Chem.* **1992**, *434*, 123.

0276-7333/94/2313-4300$04.50/0

Results and Discussion

$[Fe_3(CO)_{11}]^{2-}$ displaced a chlorine atom from ClHg(m) to afford the anionic mixed-metal clusters $[Fe_3(CO)_{10}(\mu\text{-CO})(\mu\text{-Hg(m)})]^-$ (m = $Mo(CO)_3Cp$ (**1**), $W(CO)_3Cp$ (**2**), $Fe(CO)_2Cp$ (**3**), $Mn(CO)_5$ (**4**), $Co(CO)_4$ (**5**)) in good yields (eq 1). They were isolated as their PPh_4^+ salts and are

$$[Fe_3(CO)_{11}]^{2-} + ClHgm \longrightarrow \left[\begin{array}{l} CO \\ (CO)_3Fe \quad Fe(CO)_3 \\ Fe(CO)_4 \\ Hg \\ | \\ m \end{array} \right]^- + Cl^- \quad (1)$$

red, crystalline, and relatively air-stable solids, but their solutions decompose slowly under nitrogen at room temperature. Unfortunately, all attempts to obtain suitable single crystals for X-ray diffraction studies were unsuccessful. The ν(CO) IR pattern for **1**–**5** is similar for all of them, showing, along with the bands due to the m fragments, those attributable to the $Fe_3(CO)_{11}$ moiety. In particular, the highest-wavenumber band is shifted by *ca.* 120 cm^{-1} to higher frequencies when compared with the starting iron anion. The band at *ca.* 1740 cm^{-1} indicates the presence of a bridging carbonyl ligand in all cases. The clear analogy between the infrared spectra of **1**–**5** and that reported for $(PPh_4)[Fe_3(CO)_{10}(\mu\text{-CO})(\mu\text{-AuPPh}_3)]$ suggests a similar metal framework for these clusters. This conclusion is also deduced from elemental analysis, FAB spectrometry, and electronic spectra. The FAB mass spectra of the negative ions of **1**–**5** were recorded using 3-nitrobenzyl alcohol (NBA) as the matrix. The pattern shown in all these spectra is similar and consists of the parent molecular ion in high abundance along with fragments resulting from stepwise loss of carbonyl from the parent ion, M – nCO (n = 1–3). Furthermore, the following peaks coming from the fragmentation of the starting cluster are also present: M – Hg – 3CO, M – Hgm (*i.e.* $Fe_3(CO)_{11}$), and other lighter units derived from the degradation of the last fragment. The most important conclusion about the FAB spectra is that the presence of the parent molecular ion in all of them unambigously confirms the nature of clusters **1**–**5**.

Complexes **1**–**5** display UV/vis absorption bands around 570 nm, which may be attributed to transitions between orbitals involved in the metal–metal bonds.[10] In particular, given the external localization of m fragments, no dramatic changes are seen when comparing the most ($Fe(CO)_2Cp$, 567 nm) to the least nucleophilic fragment ($Co(CO)_4$, 576 nm). An interesting aspect of the chemical reactivity of clusters containing mercury-ligand fragments is the possibility of redistribution reactions in which capped, bridged, or terminal linked derivatives are converted to the corresponding symmetric compounds. It has been discussed that the stability of the asymmetric over the symmetric compounds in this general equilibrium

$$2\ [M_m(CO)_n(HgY)] \rightleftharpoons [(M_m(CO)_n)_2Hg] + HgY_2$$

depends on the properties of both the metal cluster (particularly, its charge) and the ligand Y coordinated to the mercury center. Thus, to suppress the symmetrization of an asymmetric transition metal–mercury cluster, the ligand Y should be a highly electronegative fragment[2] (which implies a great Hg–Y bond energy). On the other hand, the presence of some negative charge on the asymmetric species appears to stabilize them toward the symmetrization by precluding the bimolecular, associative process (believed to proceed through a four-center bridged transition state) proposed for this type of reaction.[11,12]

We have observed that **1**–**5** are stable toward the redistribution reaction because in no case did we detect traces of the symmetric cluster $[\{Fe_3(CO)_{11}\}_2Hg]^{2-}$, reported by Vahrenkamp[13] while this work was in progress. The inertness of **1**–**5** compares well with that recently found for the anionic clusters $[Mn_3(CO)_{12}(\mu\text{-H})(\mu\text{-Hg(m)})]^-$,[14] again confirming that the negative charge contributes to the final stability of those metal clusters which incorporate mercury-ligand units.[15]

Although the Mössbauer spectra of neutral trinuclear iron carbonyl clusters have proven very useful in determining their structural and electronic properties,[16] there are fewer reports concerning the related anionic metal clusters.[17] The Mössbauer spectra for this type of compound are particularly interesting because they provide information about the electronic density of the different iron sites in the cluster and about their asymmetry. Thus, a correlation has been found between the isomer shift and localized negative charge in a series of comparable compounds, showing that an increase in the negative anionic charge produces a decrease in the isomer shift as a result of increased 4s electron density at the iron nucleus.[18] On the other hand, the quadrupole splitting provides a measure of the asymmetry of the electronic environment about each iron site. Although it has been established that the Mössbauer parameters of complexes are sensitive primarily to changes in the immediate environment of the Mössbauer atom,[19] we examined the electronic changes in iron atoms that could occur in the series $[Fe_3(CO)_{10}(\mu\text{-CO})(\mu\text{-Hg(m)})]^-$ as the nature of m was varied. The Mössbauer spectra of **1**–**3** and **5** were measured at 80 K, but even at this temperature, complex **4** decomposed during the data collection. The fitted Mössbauer parameters are summarized in Table 1. Except for **3**, all the spectra show the superposition of two quadrupolar doublets (Figure 1) indicating the presence of two types of iron atoms, Fe(1,2) and Fe(3). The ratio of the areas of these doublets is approximately 2:1. The spectrum of **3** displays an unusual superposition of three doublets

(10) Gladfelter, W. L.; Geoffroy, G. L. *Adv. Organomet. Chem.* **1980**, *18*, 207.

(11) Reina, R.; Rossell, O.; Seco, M. *J. Organomet. Chem.* **1990**, *398*, 285.

(12) Abraham, M. H. In *Comprehensive Chemical Kinetics*; Bamford, C. H., Tipper, C. F. H., Eds.; Elsevier: Amsterdam, 1973; Vol. 12.

(13) Deck, W.; Powell, A. K.; Vahrenkamp, H. J. *Organomet. Chem.* **1992**, *428*, 353.

(14) Rossell, O.; Seco, M.; Segalés, G.; Alvarez, S.; Pellinghelli, M. A.; Tiripicchio, A. *Organometallics* **1994**, *13*, 2205.

(15) A reviewer has suggested an alternative explanation for the nonobservance of symmetrization reactions based on steric problems as the molecules approach.

(16) Grandjean, F.; Long, G. J.; Benson, C. G.; Russo, U. *Inorg. Chem.* **1988**, *27*, 1524 and references therein.

(17) (a) Long, G. J.; O'Brien, J. F. *Hyperfine Interact.* **1988**, *40*, 101. (b) Buhl, M. L.; Long, G. J., O'Brien, J. F. *Organometallics* **1993**, *12*, 283.

(18) Collins, M. P.; Spalding, T. R.; Deeny, F. T.; Longoni, G.; Pergola, R.; Venäläinen, T. *J. Organomet. Chem.* **1986**, *317*, 243.

(19) Koreez, L. *Mössbauer Spectroscopy*; Elsevier Scientific: Amsterdam, 1979.

Table 1. ^{57}Fe Mössbauer Hyperfine Parameters (at 80 K) for Compounds 1–3 and 5

compd	site	IS[a] (δ) (mm s^{-1})	QS (Δ) (mm s^{-1})	line width (Γ) (mm s^{-1})	rel area (%)
1	Fe(1,2)	−0.016	1.366	0.239	61
	Fe(3)	−0.074	0.178	0.303	39
2	Fe(1,2)	−0.018	1.472	0.252	57
	Fe(3)	−0.097	0.242	0.382	43
3	Fe(1,2)	−0.037	1.469	0.236	58
	Fe(3)	−0.088	0.302	0.372	22
	Fe(4)	0.410	1.023	0.251	20
5	Fe(1,2)	−0.016	1.262	0.254	55
	Fe(3)	−0.060	0.190	0.374	45

[a] Isomer shift values are referred to metallic iron at room temperature.

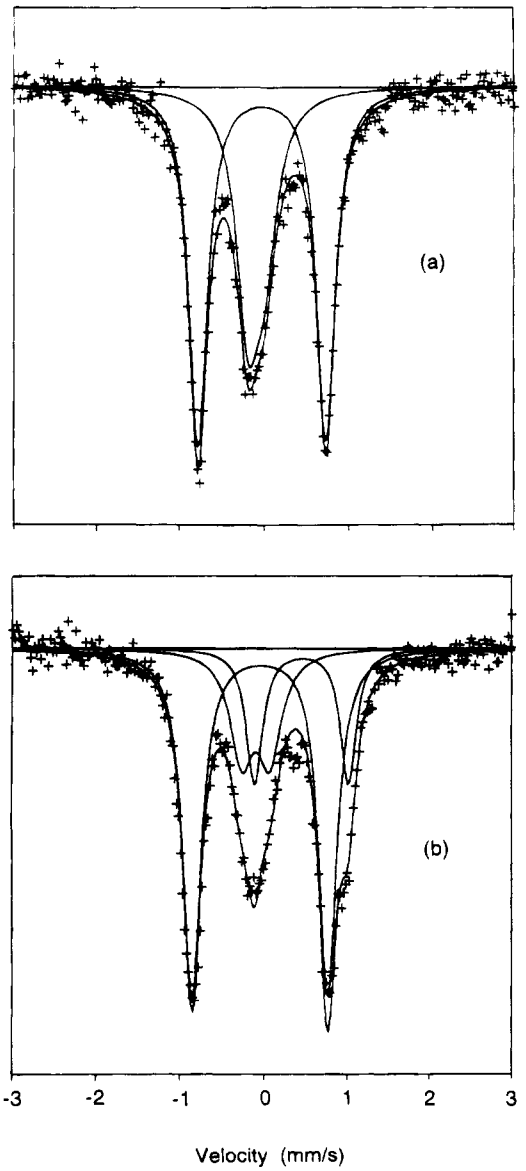

Figure 1. ^{57}Fe Mössbauer spectra of **1** (a) and **3** (b).

(Figure 1) in accordance with the presence of three nonequivalent iron nuclei. The most remarkable features of these spectra can be summarized as follows: (i) The similarity of the spectra of **1**–**3** and **5** and that reported for the NEt_4^+ salt of the anion $[Fe_3(CO)_{11}(\mu\text{-}H)]^-$ [20] suggests that both types of compound display a similar structure, as expected, taking into account the

(20) King, R. B.; Chorghade, G. S.; Bhattacharyya, N. K.; Holt, E. M.; Long, G. J. *J. Organomet. Chem.* **1991**, *411*, 419.

Table 2. Electrochemical Data (Cyclic Voltammetry and Stationary Conditions) for Complexes 1–5[a]

	oxidation						reduction		
compd	$E^{\circ\prime}$ (V)	$E_{p,a}$ (V)	ΔE (mV)	$i_{p,c}/i_{p,a}$	P (mV)	n	$E_{p,ox}$ (V)	$E_{p,red}$ (V)	n
1	0.24	0.29	91	0.98	73.4	1	−1.40	−0.09	2
2	0.25	0.30	88	0.87	83.7	1	−1.32	−0.06	2
3	0.20	0.24	83	0.80	78.4	1	−1.60	−0.93	2
4	0.28	0.32	86	0.91	61.9	1	−1.44	−0.06	2
5	0.38	0.42	87	0.98	70.3	1	−1.00	0.20	2

[a] P = slope of the linear regression of $E = \log |i_d - i/i|$; $\Delta E = E_{p,backward} - E_{p,forward} = E_{p,red} - E_{p,ox}$; n = number of electrons exchanged. Data for cyclic voltammetry are referred to a scan rate of 0.1 V s^{-1}; data for stationary conditions are referred to a Pt rotating electrode at 1000 T/min.

isolobal relationship between H^+ and $Hg(m)^+$.[21] (ii) The isomer shift of the Fe(1,2) sites is more negative than that corresponding to the Fe(3) site, revealing that the negative charge is predominantly localized to Fe(1,2) sites. This is in good accord with the observations that the formal substitution of a CO bridging group from $Fe_3(CO)_{12}$ for a hydride to give the anion $[Fe_3(CO)_{11}(\mu\text{-}H)]^-$ is accompanied by a decrease in the isomer shift of the Fe(1,2) sites.[22] What is not clear is why the presence of the $HgFe(CO)_2Cp$ fragment in **3** produces the highly negative value of the isomer shift for the Fe(3) site. (iii) The negative values of the isomer shift for Fe(1,2,3) in **1**–**3** and **5** are in clear contrast with those reported for the $[Fe_3(CO)_{11}(\mu\text{-}H)]^-$. This finding indicates that the Hg(m) fragments delocalize the negative charge on the iron sites less strongly than H^+ does. In conclusion, the formal substitution of H^+ in $[Fe_3(CO)_{11}(\mu\text{-}H)]^-$ for the $Hg(m)^+$ fragments produces notable variations in the Mössbauer spectrum, mainly in the isomer shift.

On the other hand, we believe that the slight changes in the parameters on going from **1** to **5** are better explained by distortions in the symmetry because of packing forces affecting the atomic positions than by differences in the electronic distribution of the nucleus of the metal skeleton.

Electrochemical and EPR Studies. The electrochemical properties of the title compounds were studied in the electroactivity range of the solvent (CH_2Cl_2). The voltammograms showed three electrode processes. All the studied compounds **1**–**5** exhibit the following: (i) a well-defined wave around +0.3 V corresponding to an oxidation process; (ii) an irreversible oxidation wave at +1.0 V; (iii) an irreversible reduction process around −1.4 V depending on the nature of m. The first wave around +0.3 V appears reversible if the potential sweep is restricted to the range of this electrochemical process. Data for the oxidation of the compounds are summarized in Table 2. A cyclic voltammogram of $[PPh_4][Fe_3(CO)_{10}(\mu\text{-}CO)(\mu\text{-}Hg\{Mo(CO)_3Cp\})]$ is displayed in Figure 2 as representative of all compounds. The electron transfer rate constant k° determined by the Nicholson and Shain method using a Technic[23] ultramicroelectrode is approximately 10^{-2} cm s^{-2}, this value being typical of a quasi-reversible process.[24]

The linear voltammograms at a rotating Pt disk electrode show a well-developed wave with the appear-

(21) Braunstein, P.; Rosé, J.; Tiripicchio, A.; Tiripicchio Camellini, M. *J. Chem. Soc., Dalton Trans.* **1992**, 911.
(22) Erickson, N. E.; Fairhall, A. W. *Inorg. Chem.* **1965**, *4*, 1320.
(23) (a) Nicholson, R. S. *Anal. Chem.* **1965**, *36*, 1351. (b) Nicholson, R. S.; Shain, I. *Anal. Chem.* **1966**, *37*, 706.
(24) Delahay, P. *J. Am. Chem. Soc.* **1953**, *75*, 1430.

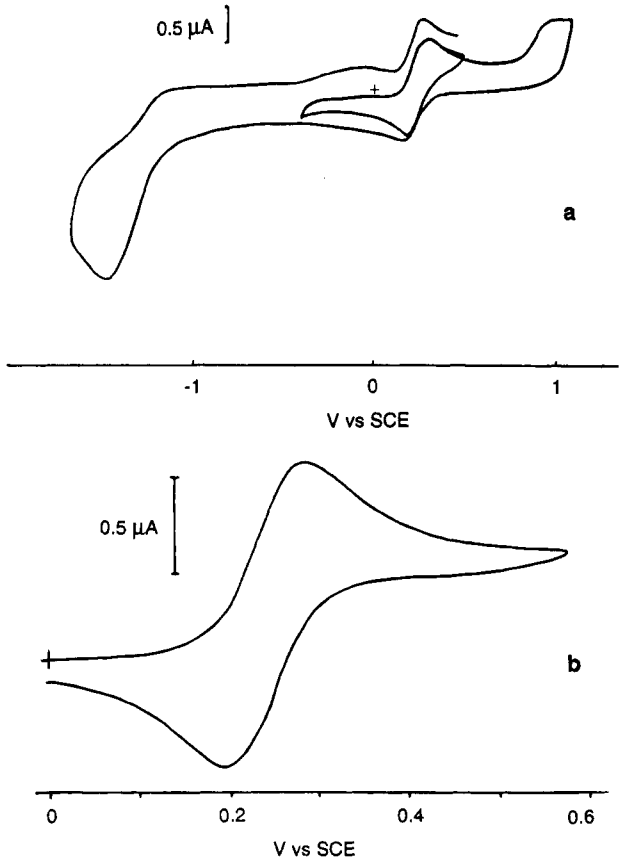

Figure 2. Ambient temperature cyclic voltammogram of **1** in CH_2Cl_2 measured at a platinum-bead electrode at a scan rate of 0.1 V s^{-1}: (a) Full scan; (b) scan for the reversible oxidation.

ance of a slow electron transfer according to the nature of the electrode surface. We observed some passivation phenomena, especially when the potential sweeps the whole electroactivity range. Similar observations are found when Pt is replaced by Au or a carbon disk. The study of the variation of the limiting currents as a function of the complex concentration, or as a function of the square root of the electrode rotation speed, shows a deviation from linearity for a diffusion-controlled process. Taking into account that CH_2Cl_2 is a nondissociative, nondonor solvent, these observations indicate the presence of a chemical reaction after the oxidation. This agrees with the quasi-reversibility of the process suggested by the cyclic voltammetry.

Controlled potential coulometry at 0.5 V using a platinum gauze electrode at −40 °C in CH_2Cl_2–[*n*-Bu_4N][PF_6] medium indicated that one electron is exchanged. During this time the dark red solution changes to deep orange. The frozen-glass EPR spectra of the latter solution show a single resonance flanked by mercury satellites (vide infra). We should point out that on heating of the orange solution to room temperature it turned green and showed no EPR signal. The IR spectra of these last solutions showed bands attributable to $Fe_3(CO)_{12}$ and $Hg(m)_2$ by comparison with the authentic samples, so we conclude that a decomposition reaction follows the electrochemical process. These results agree with those found for dinuclear iron clusters[25] and can be summarized according to an EC scheme: an electrode reaction, eq 2(E), followed by a

$$\text{(E)}\quad \underset{\textbf{1-5}}{[Fe_3(CO)_{10}(\mu\text{-}CO)(\mu\text{-}Hgm)]^-} \underset{+e^-}{\overset{-e^-}{\rightleftharpoons}} \underset{\textbf{1'-5'}}{[Fe_3(CO)_{11}(Hgm)]^{\bullet}} \quad (2)$$

$$\text{(C)}\quad \underset{\textbf{1'-5'}}{[Fe_3(CO)_{11}(Hgm)]^{\bullet}} \longrightarrow Fe_3(CO)_{12} + Hgm_2 + \text{products} \quad (3)$$

single chemical reaction, eq 3 (C). The second oxidation process at +1.0 V is observed for all the $(PPh_4)[Fe_3(CO)_{10}(\mu\text{-}CO)(\mu\text{-}Hg(m))]$ complexes. It probably corresponds to the oxidation of a product formed during the first step, which led to the fragmentation of the neutral cluster; this new oxidation step was not further studied.

As pointed out above, an irreversible reduction process occurred in the region around −1.4 V. The height of the wave is double in intensity compared to that observed for the oxidation step. An exhaustive controlled potential electrolysis confirmed that two electrons were exchanged. In the reverse scan the voltammograms showed an additional peak, the position of which depends on the nature of m. For example, when m = $[Co(CO)_4]^-$, a reverse peak was observed at 0.2 V on the voltammogram. This was attributed to the oxidation of the resulting $[Co(CO)_4]^-$ formed during the reduction of **5**. Moreover, the addition of an authentic sample of $Na[Co(CO)_4]$ increased the peak. For complexes **1** and **2** the reverse peak is observed at −0.09 and −0.06 V, respectively. These were attributed to the reoxidation of the species $[Mo(CO)_3Cp]^-$ and $[W(CO)_3Cp]^-$ generated during the reduction step of **1** and **2**.[26] Compounds **3** and **4** also showed this process, and data are collected in Table 2. In view of these findings, we conclude that an electrochemical step occurs followed

$$[Fe_3(CO)_{10}(\mu\text{-}CO)(\mu\text{-}Hgm)]^- + 2e^- \rightleftharpoons [Fe_3(CO)_{11}Hgm]^{3-}$$

by a cleavage of the trianionic species, which finally decompose, especially in mononuclear anionic fragments, m^-, which were identified. These results agree with those found in the literature on the study of trimetallic $Hg(m)_2$ and tetrametallic Pt_2M_2 complexes.[27,28]

The X-band EPR spectrum in CH_2Cl_2 is identical for all complexes (Figure 3) and consists of a single strong resonance centered at *ca.* 3267 G (g = 2.06) flanked by two satellite signals assigned to a hyperfine coupling with ^{199}Hg (I = $^1/_2$, natural abundance 16.84%) with $a(^{199}Hg)$ = 181 G. Moreover, the presence of the two additional weaker signals (marked with asterisks) in the spectrum may indicate another hyperfine coupling with the ^{201}Hg isotope (I = $^3/_2$, natural abundance 13.22%). The complete splitting is not visible because the two central lines of the quadruplet lie inside the main resonance. Using this assumption, a hyperfine constant value of $a(^{201}Hg)$ = 105 G is obtained. The hyperfine

(25) Baker, R. T.; Calabrase, J. C.; Krusic, P. J.; Therien, M. J.; Trogler, W. C. *J. Am. Chem. Soc.* **1988**, *110*, 8392. Dessy, R. E.; Pohl, R. L.; King, R. B. *J. Am. Chem. Soc.* **1966**, *88*, 5121 and references therein.
(26) Kadish, K. M.; Lacombe, D. A.; Anderson, J. E. *Inorg. Chem.* **1986**, *25*, 2246.
(27) Lemoine, P.; Giraudeau, A.; Gross, M.; Braunstein, P. *J. Chem. Soc., Chem. Commun.* **1980**, 77.
(28) Jund, R.; Lemoine, P.; Gross, M.; Bender, R.; Braunstein, P. *J. Chem. Soc., Chem. Commun.* **1983**, *86*.

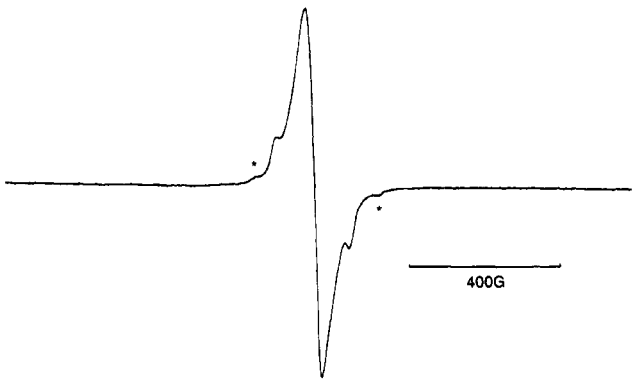

Figure 3. X-band EPR spectrum of **4'** in CH_2Cl_2 at 100 K. The signals marked with asterisks correspond to the large hyperfine coupling with the ^{201}Hg isotope ($I = {}^3/_2$, natural abundance 13.22%).

splitting value for ^{199}Hg is in agreement with those found in literature.[29-33] Additionally, the corresponding value for ^{201}Hg compares quite well with the only one reported for this kind of compound.[29] The quadrupole effect of the ^{201}Hg nucleus causes the magnitudes of the hyperfine coupling constants of both mercury isotopes to not mirror the ratio of their nuclear magnetogyric constants. Krusic et al.[25,34-36] detected ^{57}Fe satellite lines ($I = {}^1/_2$, natural abundance 2.2%) in dinuclear iron complexes. They found hyperfine coupling values ranging from 3.5 to 13 G. These signals were not observed in our spectra, although their presence may have been masked by the broad resonance.

Since the width of the main resonance is the same in all spectra and no other hyperfine coupling is observed, we deduce that the other active nuclei of the "m" fragments (m = $Mo(CO)_3Cp$, $W(CO)_3Cp$, $Fe(CO)_2Cp$, $Mn(CO)_5$, $Co(CO)_4$) are not involved in the delocalization of the unpaired electron. Bearing all this in mind, it appears that the unpaired electron density in the neutral radical is primarily located in the metallic core, formed by three iron atoms and one mercury atom. The $a(^{199}Hg)$ value found indicates that s-type orbitals owing to the mercury atom make a significant contribution to the SOMO.

Experimental Section

All manipulations were performed under an atmosphere of prepurified N_2 with use of standard Schlenk techniques, and all solvents were distilled from appropriate drying agents. Elemental analyses of C and H were carried out at the Institut de Bio-Orgànica de Barcelona. Infrared spectra were recorded in THF solutions on a Nicolet FT-IR 520. ^1H NMR and ^{13}C NMR were obtained on a Varian XL-200 spectrometer (δ(TMS) = 0.00 ppm). UV–vis spectra were recorded in CH_2Cl_2 solutions on a Shimadzu UV-160A. FABS(−) spectra were recorded on an Autospec U, Cs^+, 30 kV, NBA matrix. $[PPh_4]_2[Fe_3(CO)_{11}]$[37] and ClHg(m) (m = $Mo(CO)_3Cp$, $W(CO)_3Cp$, $Fe(CO)_2Cp$, $Mn(CO)_5$, $Co(CO)_4$)[9a] were prepared as described previously.

Synthesis of $[PPh_4][Fe_3(CO)_{10}(\mu\text{-}CO)(\mu\text{-}Hg\{Mo(CO)_3Cp\})]$ (1). Details of the synthesis of **1** also apply to **2**–**5**. A solution of $ClHgMo(CO)_3Cp$ (0.38 g, 0.77 mmol) in THF (20 mL) was added dropwise to a previously cooled suspension of $[PPh_4]_2[Fe_3(CO)_{11}]$ (0.89 g, 0.77 mmol) in THF (40 mL) at −15 °C. The mixture turned dark red immediately. After 30 min of stirring, the mixture was filtered off to eliminate PPh_4Cl and the red solution was evaporated to dryness. The remaining solid was extracted with methanol (3 × 20 mL), the mixture was filtered again to ensure all PPh_4Cl had been removed, and the solvent was reduced to 20 mL. Cooling this solution to −30 °C overnight resulted in the deposition of **1** (0.46 g) as a dark red crystals. An additional 0.17 g of the product complex was obtained by concentration and cooling of the mother liquor. The total yield was 65%.

FABS (M^-): *m/e* 921. IR (THF, cm^{-1}): ν(CO) stretch 2054 s, 1991 vs, 1964 s, 1893 s, 1877 s, 1750 m. ^1H NMR (25 °C, acetone-d_6, δ(ppm)): 5.56 (s, 5H, C_5H_5). ^{13}C NMR (25 °C, acetone-d_6, δ(ppm): 87.8 (s, C_5H_5). UV (CH_2Cl_2) (λ_{max}/nm): 288, 346 (sh), 571. Anal. Calcd for $C_{43}H_{25}Fe_3HgMoO_3P$: C, 40.95; H, 1.98. Found: C, 41.22; H, 2.01.

$[PPh_4][Fe_3(CO)_{10}(\mu\text{-}CO)(\mu\text{-}Hg\{W(CO)_3Cp\})]$ (2). Yield: 0.63 g (60%). FABS (M^-): *m/e* 1009. IR (THF, cm^{-1}): ν(CO) stretch 2053 s, 1990 vs, 1960 s, 1886 s, 1871 s, 1749 m. ^1H NMR (25 °C, acetone-d_6, δ(ppm)): 5.67 (s, 5H, C_5H_5). ^{13}C NMR (25 °C, acetone-d_6, δ(ppm)): 88.3 (s, C_5H_5). UV (CH_2Cl_2) (λ_{max}/nm): 285, 344 (sh), 571. Anal. Calcd for $C_{43}H_{25}Fe_3HgWO_3P$: C, 38.28; H, 1.85. Found: C, 38.11; H, 1.84.

$[PPh_4][Fe_3(CO)_{10}(\mu\text{-}Hg\{Fe(CO)_2Cp\})]$ (3). Yield: 0.43 g (52%). FABS (M^-): *m/e* 855. IR (THF, cm^{-1}): ν(CO) stretch 2051 s, 1986 vs, 1948 s, 1832 s, 1748 m. ^1H NMR (25 °C, acetone-d_6, δ(ppm)): 4.92 (s, 5H, C_5H_5). ^{13}C NMR (25 °C, acetone-d_6, δ(ppm)): 79.4 (s, C_5H_5). UV (CH_2Cl_2) (λ_{max}/nm): 281, 354 (sh), 567. Anal. Calcd for $C_{42}H_{25}Fe_4HgO_2P$: C, 42.28; H, 2.10. Found: C, 42.22; H, 2.01.

$[PPh_4][Fe_3(CO)_{10}(\mu\text{-}CO)(\mu\text{-}Hg\{Mn(CO)_5\})]$ (4). Yield: 0.38 g (45%). FABS (M^-): *m/e* 873. IR (THF, cm^{-1}): ν(CO) stretch 2077 m, 2046 s, 1992 vs, 1953 s, 1753 m. UV (CH_2Cl_2) (λ_{max}/nm): 288, 341 (sh), 571. Anal. Calcd for $C_{40}H_{20}Fe_3HgMnO_5P$: C, 39.67; H, 1.65. Found: C, 39.11; H, 1.54.

$[PPh_4][Fe_3(CO)_{10}(\mu\text{-}CO)(\mu\text{-}Hg\{Co(CO)_4\})]$ (5). Yield: 0.38 g (41%). FABS (M^-): *m/e* 849. IR (THF, cm^{-1}): ν(CO) stretch 2048 s, 1995 vs, 1887 s, 1757 w. UV (CH_2Cl_2) (λ_{max}/nm): 288, 381 (sh), 576. Anal. Calcd for $C_{39}H_{20}Fe_3HgCoO_4P$: C, 39.46; H, 1.69. Found: C, 39.98; H, 1.79.

Mössbauer Measurements. The Mössbauer spectra were recorded in a transmission geometry using driving equipment of constant acceleration provided by a ^{57}Co (10 mCi) source diffused into an Rh matrix. The natural line width of this source was found to be 0.26 mm s^{-1}. Metallic iron of high purity (25 μm thick α-Fe) was used for the calibration of the velocity scale. The measurements were carried out at 80 K using a liquid-nitrogen cryostat. The Mössbauer effect absorbers were prepared in a nitrogen atmosphere. The hyperfine parameters were determined fitting the spectra by a least squares method assuming that the two Lorentzian lines of the quadrupole doublets have the same line width and different relative intensities.[38-40]

Electrochemical Measurements. Electrochemical measurements were carried out with a Dacfamov potentiostat

(29) Fullam, B. W.; Symons, M. C. R. *J. Chem. Soc., Dalton, Trans.* **1974**, 1086.
(30) Chen, K. S.; Smith, R. T.; Wan, J. K. S. *Can. J. Chem.* **1978**, *56*, 2503.
(31) Courtneidge, J. L.; Davies, A. G.; Gregory, P. S.; McGuchan, D. C.; Yazdi, S. N. *J. Chem. Soc., Chem. Commun.* **1987**, 1192.
(32) Courtneidge, J. L.; Davies, A. G.; McGuchan, D. C.; Yazdi, S. N. *J. Organomet. Chem.* **1988**, *341*, 63.
(33) Davies, A. G.; McGuchan, D. C. *Organometallics* **1991**, *10*, 329.
(34) Baker, R. T.; Krusic, P. J.; Calabrase, J. C.; Roe, D. C. *Organometallics* **1986**, *5*, 1506.
(35) Krusic, P. J.; Jones, D. J.; Roe, D. C. *Organometallics* **1986**, *5*, 456.
(36) Krusic, P. J.; Baker, R. T.; Calabrase, J. C.; Morton, J. R.; Preston, K. F.; Le Page, Y. *J. Am. Chem. Soc.* **1989**, *111*, 1262.
(37) Hodali, H. A.; Shriver, D. F. *Inorg. Synth.* **1980**, *20*, 222.
(38) Gibb, T. C. *Principles of Mössbauer spectroscopy*; Wiley: New York, 1976.
(39) Nussbaum, R. H. In *Mössbauer Effect Methodology*: Gruverman, I. J., Ed.; Plenum: New York, 1966.
(40) Güttich, P.; Link, R.; Trautwein, A. *Mössbauer Spectroscopy and Transition Metal Chemistry*; Springer: Berlin, 1978.

connected to an Apple IIe microcomputer.[41] The positive feedback (scan rate >1 V s^{-1}) or interrupt (scan rate <1 s^{-1}) method was used to minimize the uncompensated resistance (iR) drop. Electrochemical experiments were performed in an air-tight three-electrode cell connected to a vacuum argon/N_2 line. The cell was degassed and filled according to standard vacuum techniques. The reference consisted of a saturated calomel electrode (SCE) separated from the solution by a bridge compartment. The counter electrode was a spiral of ca. 1 cm^2 apparent surface area, made of a platinum wire 8 cm long and 0.5 cm in diameter. The working electrode was Pt (1 mm diameter) for cyclic voltammetry. A rotating disk electrode (RDE) with a 2 mm diameter Pt or Au disk or 3 mm diameter carbon disk (Tacussel EDI) was used for analytical purposes, and Pt foil was used for electrolysis. $E^{\circ\prime}$ values were determined as the average of cathodic and anodic peak potentials, *i.e* $[(E_{p,c} + E_{p,a})/2]$. The supporting electrolyte $[n\text{-}Bu_4N][PF_6]$ (Aldrich analytical grade) was used as received. Dichloromethane (SDS purex) was freshly distilled over $CaCl_2$ and then P_2O_5 prior to use. The solutions used during the electrochemical studies were typically 4×10^{-4} M in the organometallic complex and 0.1 M in $[n\text{-}Bu_4N][PF_6]$. In the same conditions ferrocene is oxidized at $E^{\circ\prime} = 0.42$ V *vs* SCE and the peak potential separation ΔE is 60 mV. For complexes **1**–**5** the current peak ratio $i_{p,c}/i_{p,a}$ values are 1 ($i_{p,a}$ and $i_{p,c}$ are the anodic and cathodic peak currents) at a 2 V s^{-1} scan rate. The changes observed in $i_{p,a}/v^{1/2}$ ratios with the voltage scan rate are indicative of a chemical or kinetic complication. Due to the experimental requirements (temperature and atmosphere control) a particular electrolysis cell[42] allowing combined coulometry–EPR studies was used successfully.

EPR Measurements. EPR spectra were obtained in a Bruker ESP 300 E in the X-band mode at 100 K with the standard Bruker VT 1000 cryostat. The compounds **1′**–**5′** were prepared by electrolysis of complexes **1**–**5**, respectively, in CH_2Cl_2 (typical concentrations were 4×10^{-4} M). A portion of these solutions was then transferred by syringe from the electrolytic cell into a precooled EPR tube and immediately frozen by immersion in liquid nitrogen just before recording the EPR spectrum.

Acknowledgment. We thank J. Tejada for facilitating access to the Mössbauer spectrometer and A. Mari for recording EPR spectra. Financial support was generously provided by the DGICYT (Project PB90-0055-C02-01).

OM940305K

(41) Cassoux, P.; Dartiguepeyron, R.; Fabre, P. L.; de Montauzon, D. *Actual Chim.* **1985**, *1–2*, 79; *Electrochim. Acta* **1985**, *30*, 1485.

(42) Cros, G.; Costes, J. P.; de Montauzon, D. *Polyhedron* **1984**, *3*, 585.